Electronic Supplementary Material (ESI) for Physical Chemistry Chemical Physics.

Dielectric switching in corelation to the structural phase transitions in tetrapropylammonium perchlorate.

Monika Trzebiatowska[a], Dorota A. Kowalska[a], Marek Gusowski[b]*, Ewelina Jach[b], Agnieszka Ciżman[b]

[a]*Institute of Low Temperature and Structure Research, Polish Academy of Sciences, 50-422 Wrocław, Poland*

[b]*Faculty of Fundamental Problems of Technology, Wrocław University of Science and Technology, Wybrzeże Wyspiańskiego 27, 50-370, Wrocław, Poland*

*corresponding author; e-mail: marek.gusowski@pwr.edu.pl

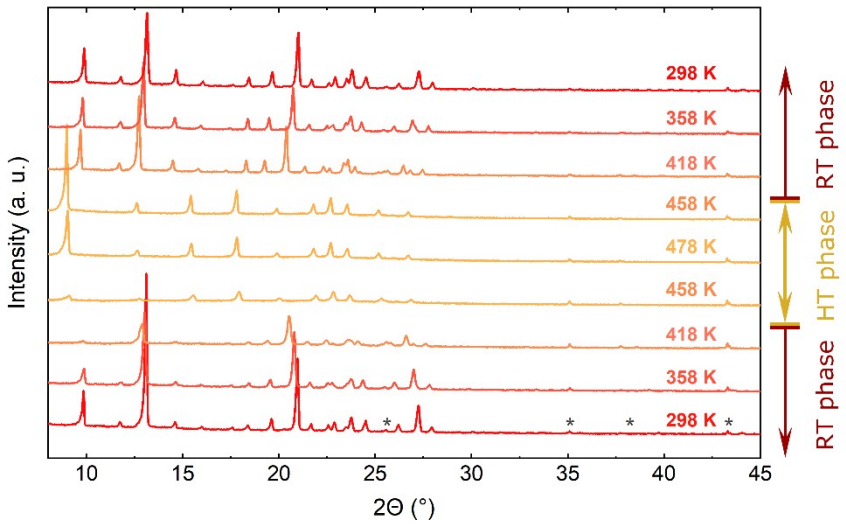

Fig. S1. The Set of PXRD diagrams showing reversible RT ↔ HT phase transition in $TePrAClO_4$. The intensities marked with asterisks are from Al_2O_3 in the sample holder and are present in all shown diffraction patterns.

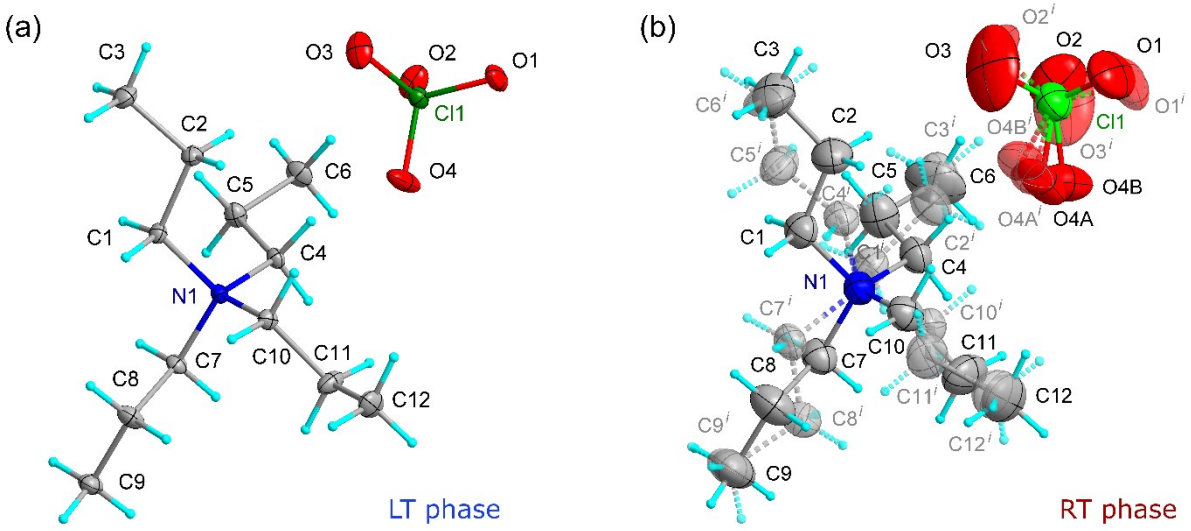

Fig. S2. The comparison of the asymmetric units of $TePrAClO_4$ in LT phase (a) and in RT phase (b). The atom numbering scheme is shown. Symmetry code: (i) *x*, *y*, −*z*+1/2. All non-hydrogen atoms are shown in ellipsoid representation at 40% probability level.

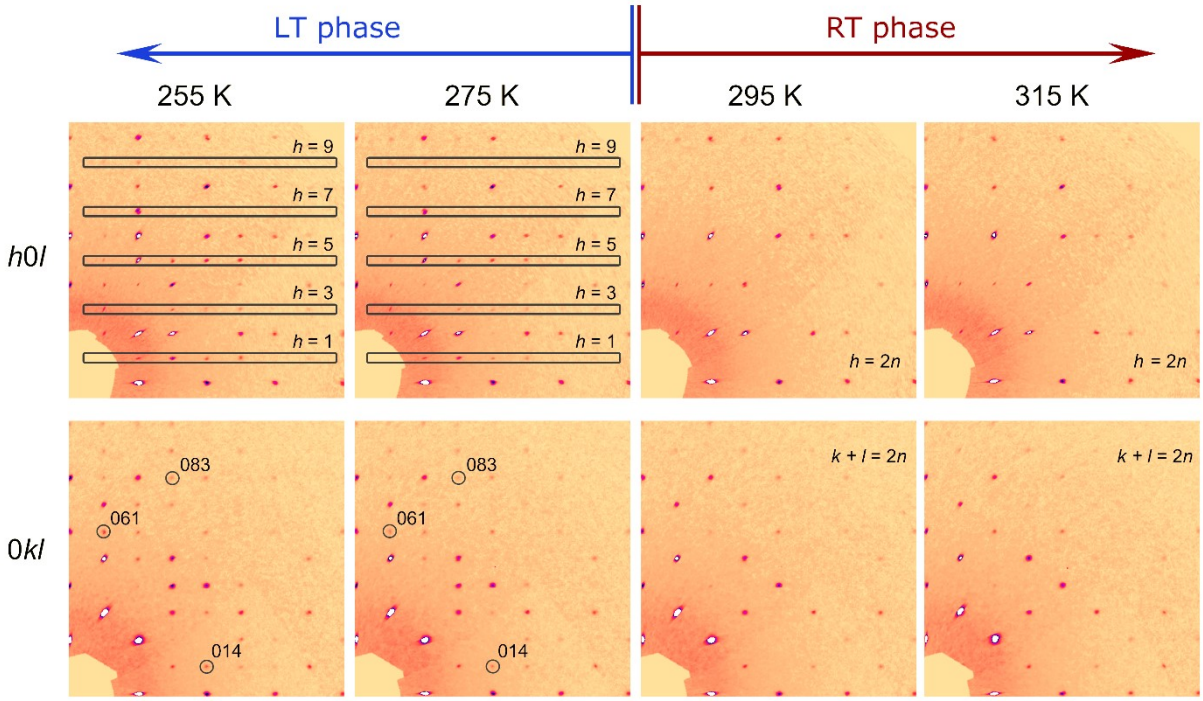

Fig. S3. The sections of the reciprocal space confirming the structural phase transition (PT1). The additional Bragg peaks appear below PT1 (some of them are edged with black).

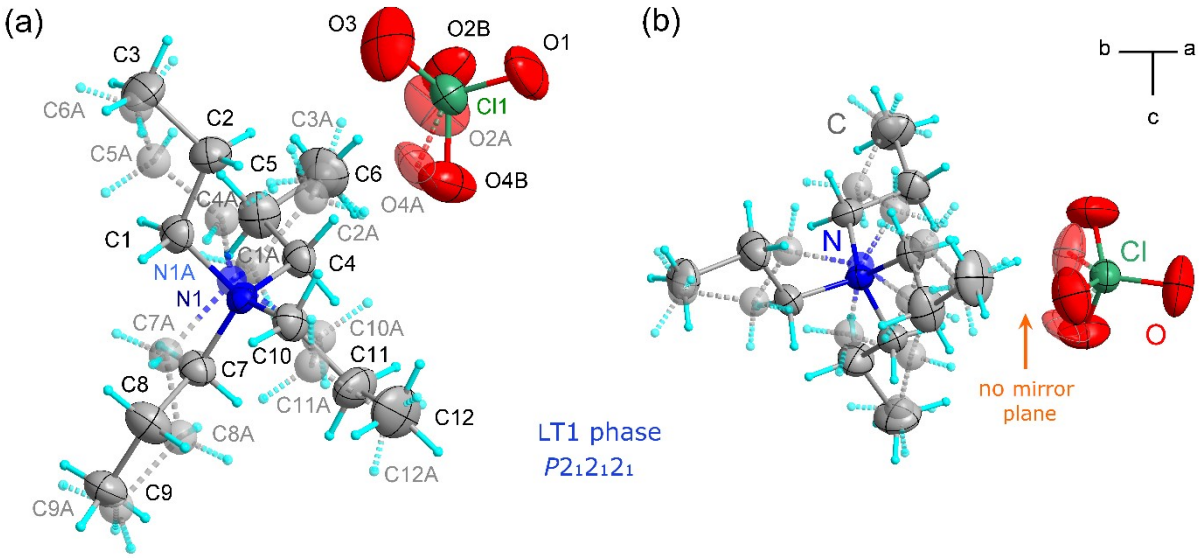

Fig. S4. (a) The asymmetric unit of $TePrAClO_4$ in LT1 phase at 275 K. (b) The absence of a mirror plane (perpendicular to the *c* crystallographic direction) below PT1 in LT1 phase is designated by an arrow. Non-hydrogen atoms are shown in ellipsoid representation at 40% probability level, except atoms belonging to the disordered moiety (11% of all $TePrA^+$ cations) which are shown in standard representation.

Table S1. Diffraction experimental details for LT1 phase of $TePrAClO_4$.

M_r = 285.80, Z = 4; chemical formula: $ClO_4 \cdot (C_3H_7)_4N$; crystal form: block; crystal colour: colourless; numerical absorption correction based on gaussian integration over a multifaceted crystal model was applied; empirical absorption correction using spherical harmonics, implemented in SCALE3 ABSPACK scaling algorithm; all H-atom parameters were constrained.

Phase	**LT1**
Crystal data	
Crystal system	Orthorhombic
Space group	$P2_12_12_1$ (no. 19)
Temperature (K)	275
a, b, c (Å)	13.548(3), 12.230(3), 9.700(2)
V(Å^3)	1607.2(9)
μ (mm^{-1})	0.25
Crystal size (mm)	0.24 × 0.13 × 0.10
Data collection	
Refl. measured/ unique/observed [$I > 2\sigma(I)$]	17869/ 3856/ 2340
R_{int}	0.040
$(\sin \theta/\lambda)_{max}$ (Å^{-1})	0.668
Refinement	
$R[F^2 > 2\sigma(F^2)]$, $wR(F^2)$, S	0.048, 0.114, 1.01
Data/ parameters / restraints	3856/ 243/ 13
$\Delta\rho_{max}$, $\Delta\rho_{min}$ (e Å^{-3})	0.20, -0.27
Absolute structure	Refined as a 2-component inversion twin
Abs. struct. param.	0.55 (12)

Table S2. Selected hydrogen bond parameters for $TePrAClO_4$.

	Temp.	*D*—H···*A*	*D*—H (Å)	H···*A* (Å)	*D*···*A* (Å)	*D*—H···*A* (°)
RT phase	295 K	C1—H1*B*···O1^{i}	0.97	2.70	3.662 (5)	171
		C1—H1*A*···O3^{ii}	0.97	2.60	3.534 (5)	161
		C3—H3*C*···O1^{ii}	0.96	2.50	3.39 (2)	154
		C4—H4*A*···O4*B*	0.97	2.70	3.624 (3)	153
		C5—H5*B*···O4*B*^{i}	0.97	2.52	3.182 (5)	126
		C6—H6*C*···O1^{iii}	0.96	2.61	3.28 (2)	127
		C7—H7*B*···O3^{iii}	0.97	2.25	3.38 (2)	161
		C10—H10*A*···O4*A*	0.97	2.49	3.34 (2)	146
LT1 phase	275 K	C1—H1*B*···O3^{iv}	0.97	2.51	3.430 (6)	158
		C4—H4*A*···O2*A*	0.97	2.56	3.50 (2)	162
		C5—H5*A*···O4*A*^{v}	0.97	2.58	3.31 (2)	133
		C6—H6*C*···O1^{vi}	0.96	2.66	3.41 (2)	136
		C7—H7*A*···O2*A*^{vi}	0.97	2.57	3.53 (2)	171
		C10—H10*B*···O4*A*	0.97	2.40	3.32 (2)	159
		C3A—H3*AA*···O1^{vi}	0.96	2.74	3.40 (7)	127
		C4A—H4*AB*···O3^{iv}	0.97	2.62	3.50 (3)	150
		C5A—H5*AA*···O4*B*^{v}	0.97	2.55	3.21 (4)	126
		C7A—H7*AA*···O3^{iv}	0.97	2.56	3.45 (3)	154
		C10A—H10*D*···O4*B*	0.97	2.47	3.34 (3)	149
LT phase	100 K	C1—H1*A*···O1^{v}	0.97	2.59	3.551 (2)	170
		C1—H1*B*···O3^{iv}	0.97	2.41	3.341 (2)	160
		C4—H4*A*···O4	0.97	2.58	3.466 (2)	153
		C5—H5*B*···O4^{v}	0.97	2.57	3.409 (2)	144
		C6—H6*C*···O1^{vi}	0.96	2.60	3.318 (2)	132
		C7—H7*B*···O2^{vi}	0.97	2.52	3.469 (2)	165
		C10—H10*A*···O4	0.97	2.42	3.270 (2)	146

Symmetry codes: (i) *x*−1/2,−*y*+3/2,*z*; (ii) −*x*+1/2,*y*+1/2,−*z*; (iii) −x+1/2,*y*+1/2,*z*+1/2; (iv) −*x*+1, *y*+1/2,−*z*+1/2; (v) *x*−1/2, −*y*+3/2, −*z*; (vi) −*x*+1, *y*+1/2,−*z*−1/2.

Table S3. The observed Raman and IR modes (in cm^{-1}) of $TePrAClO_4$ and their proposed assignment.

$TePr_4AClO_4$						**Assignment**
IR			**Raman**			
80 K	**350 K**	**490 K**	**80 K**	**300 K**	**470 K**	
3010sh			3015m	3009m		$\nu_{as}CH_3$ ν_sCH_3
2999sh			2994m			ν_sCH_3
2981m	2980m	2978m	2981s	2982vs	2977s	$\nu_{as}CH_3$ $\nu_{as}CH_2$ ν_sCH_3 ν_sCH_2
2974m	2972sh		2959vs	2961s	2960s	$\nu_{as}CH_3$ $\nu_{as}CH_2$ ν_sCH_3 ν_sCH_2
2952w			2948sh	2940vs	2939vs	ν_sCH_2
2944w	2945w	2941w	2934s			$\nu_{as}CH_2$ ν_sCH_2
2920w			2928s	2923sh	2920sh	ν_sCH_2
2885m	2885w	2883w	2910m			$\nu_{as}CH_2$ ν_sCH_2
2882m			2880s	2882s	2881s	$\nu_{as}CH_2$ ν_sCH_2
2806vw			2806vw	2802vw		overtone
2796vw			2784vw	2784vw		overtone
2788vw	2784vw		2741vw		2745w	overtone
2734vw	2738vw		2734w	2739w		overtone
2534vw						combination
2448vw	2421vw					combination
2187vw	2193vw					overtone
2027vw						overtone
2014vw	2018vw	2021vw				overtone
2003vw						overtone
			1527vw			combination
1488m		1484sh	1490w			$\delta_{as}CH_3$
1480m	1479m	1476w	1481w	1485vw		$\delta_{as}CH_3$ $\delta_{as}CH_2$ δ_sCH_3 δ_sCH_2
1474m						$\delta_{as}CH_3$
1467m	1461w	1464sh	1466sh			$\delta_{as}CH_3$
			1461m	1456m	1458w	δ_sCH_2
1456m			1454m	1454sh		$\delta_{as}CH_2$ δ_sCH_2
1446w						$\delta_{as}CH_2$
1441vw						$\delta_{as}CH_2$
1409vw	1408vw		1406w	1405vw		$\delta_{as}CH_2$ δ_sCH_2
1394w	1393vw					$\delta_{as}CH_2$
1384vw	1386w	1387w				$\delta_{as}CH_2$
1376vw						$\delta_{as}CH_2$
1360vw	1359vw		1359w	1359w		ωCH_2
1337vw			1333m	1332w		ωCH_2
1331vw	1333vw	1329vw	1322sh	1318sh	1321w	ωCH_2
1317vw	1317vw		1314w	1314w		ωCH_2

1280vw	1276vw		1293vw	1293vw		tCH_2
			1194vw	1190vw		tCH_2
1176w			1174vw	1174vw		νCN
			1157vw	1153vw		νCN
			1138w	1136w	1139vw	νCN
1113s		1114sh				$\nu_{as}ClO_4^-$ (F_2)
1105s	1108sh		1105m	1102m	1102w	$\nu_{as}ClO_4^-$ (F_2)
1097vs	1096vs		1097w	1092sh		$\nu_{as}ClO_4^-$ (F_2)
1091vs	1090vs	1091vs	1090w			$\nu_{as}ClO_4^-$ (F_2)
1086vs			1086w	1088sh		$\nu_{as}ClO_4^-$ (F_2)
1077s	1079sh		1076vw			$\nu_{as}ClO_4^-$ (F_2)
1039w	1040w		1040m	1038m		νCC
			1032m	1032m	1032m	νCC
992w						ρCH_3 τCH_2
984m	983w		983vw	983vw		ρCH_3 τCH_2
969m	969w	971w	970vw	968vw		ρCH_3 τCH_2
933vw	932vw	931vw	933vs	931vs	931s	$\nu_sClO_4^-$ (A_1)
922vw	921vw		920m	916w		$\nu_sClO_4^-$ (A_1)
915vw	915sh	907vw				ρCH_3 tCH_2
904vw			903m	909m	908m	ρCH_3 tCH_2
883vw	880vw		880vw	880vw		νCC
868w	871vw	867vw	867vw	871vw	872vw	νCC
855w	852w	840vw	854w	852w	843w	νCC
774vw			774w	771w		τCH_2
761w	758w	759w	761w	759w		τCH_2
752w	752w		751vw	751vw		τCH_2
748w						τCH_2
622m	623m	623m	621w	623w	620w	$\delta_{as}ClO_4^-$ (F_2)
			517vw	516vw		δCNC
			460w			$\delta_sClO_4^-$ (E)
			456w	457w	457w	$\delta_sClO_4^-$ (E)
			420w			δCNC
			384vw			δCNC δCCC
			370vw	367vw	370vw	δCCC
			348vw	342vw		δCCC
			310m	309m	307m	$LClO_4^-$
			133sh			$T'ClO_4^-$
			126w	119w		T'TePrA
			87w	77w	65m	LTePrA

s-very strong, s-strong, m-medium, w-weak, vw-very weak; ν_s–symmetric stretching, ν_{as}-asymmetric stretching, ν_s–symmetric stretching, ν_{as}–asymmetric stretching, δ_{as}-asymmetric bending, δ_s, δ-symmetric bending (scissoring), ρ-rocking, ω-wagging, τ-twisting (torsion), T–translation, L–libration;

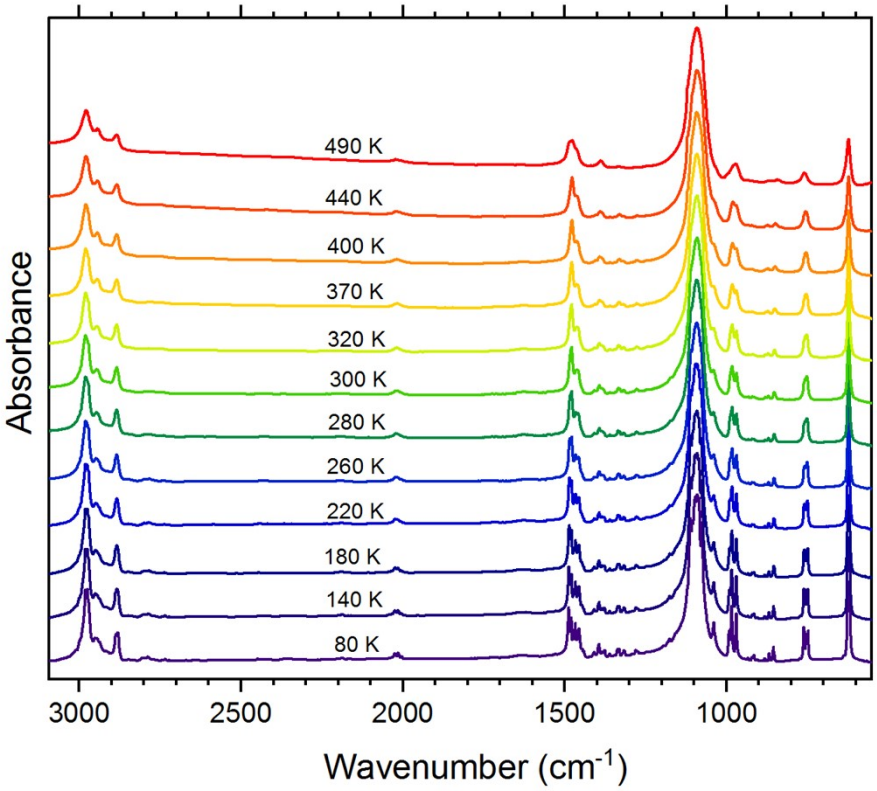

Fig. S5. The temperature-dependent IR spectra in the full wavenumber range of $TePrAClO_4$.

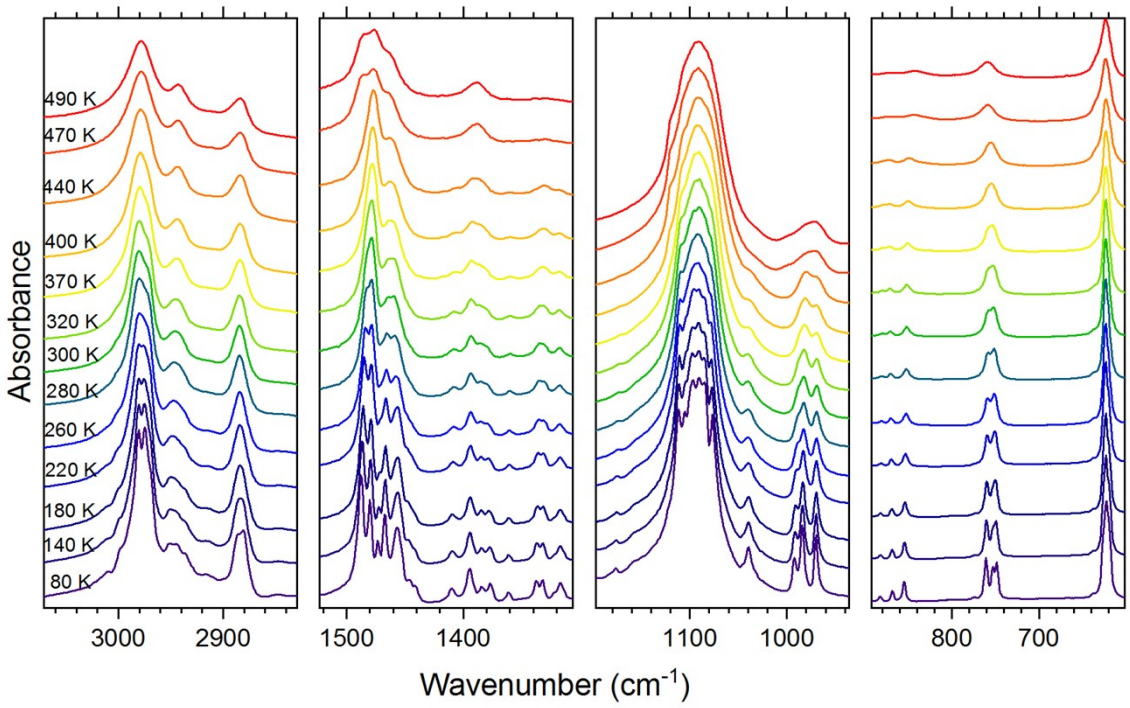

Fig. S6. The details of temperature-dependent IR spectra in the full wavenumber range of $TePrAClO_4$.

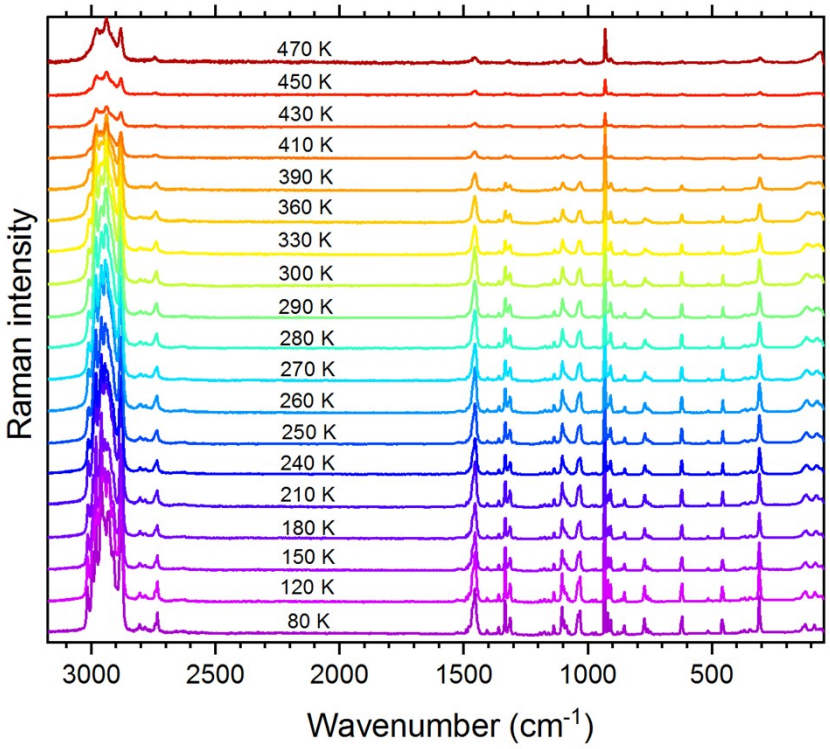

Fig. S7. The temperature-dependent Raman spectra in the full wavenumber range of $TePrAClO_4$.

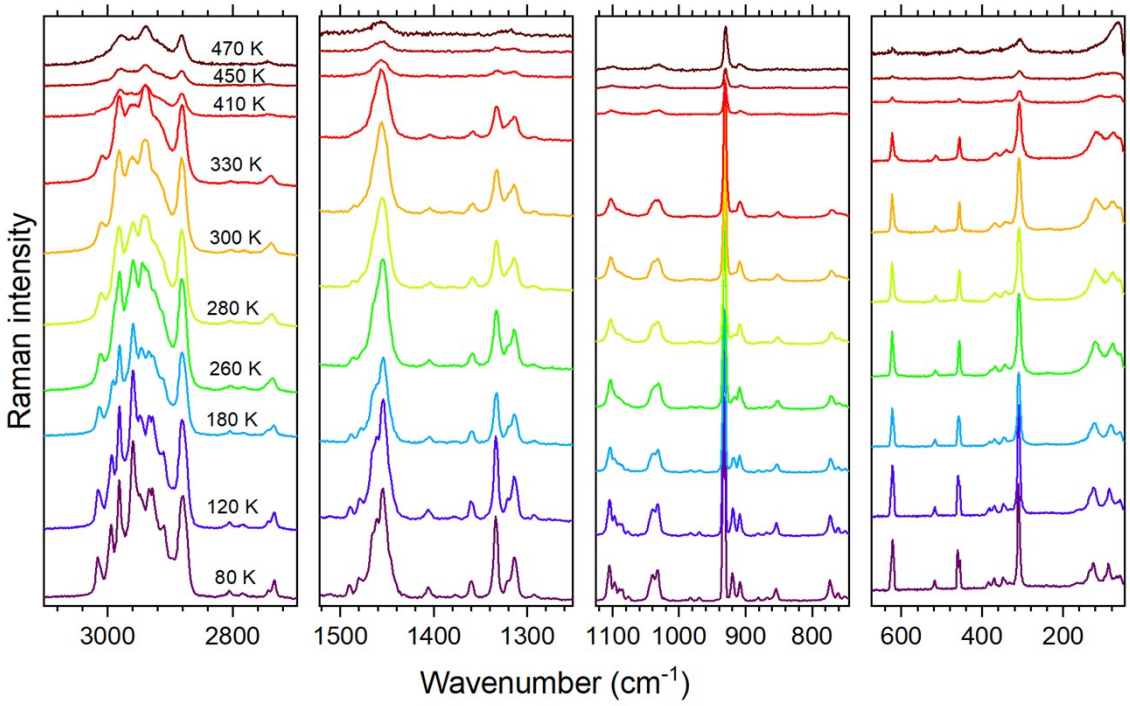

Fig. S8. The details of temperature-dependent Raman spectra in the full wavenumber range of $TePrAClO_4$.

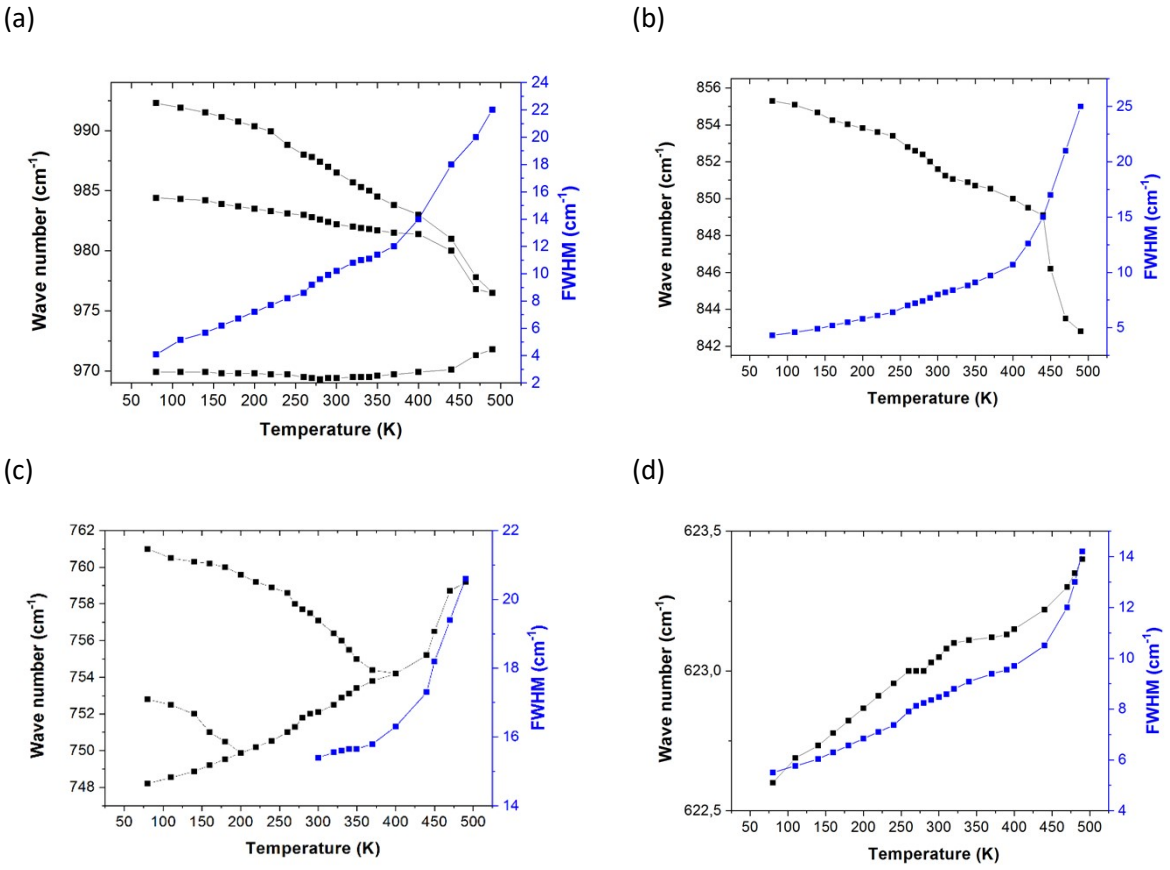

Fig. S9. The plots of the wavenumber and FWHM vs. T of the selected IR modes: (a) deformation ρCH_3 and τCH_2, (b) νCC, (c) τCH_2 and d) $\delta_{as}ClO_4^-$ (F_2) in TePrAClO_4.

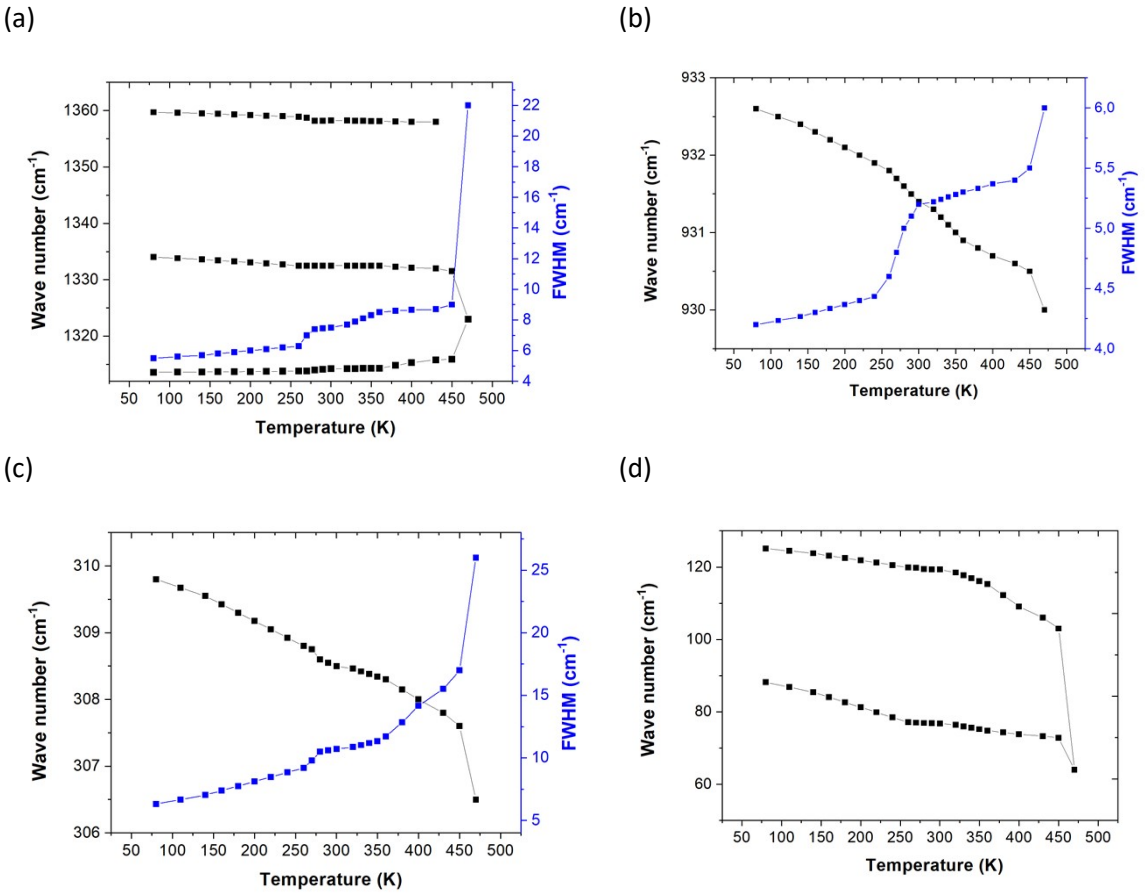

Fig. S10. The plots of the wavenumber and FWHM vs. T of the selected Raman modes: (a) ωCH_2, (b) $\nu_s ClO_4^-$ (A_1), (c) $LClO_4^-$, (d) translations $T'ClO_4^-$ and translations and librations of $TePrA^+$ cations in $TePrAClO_4$.

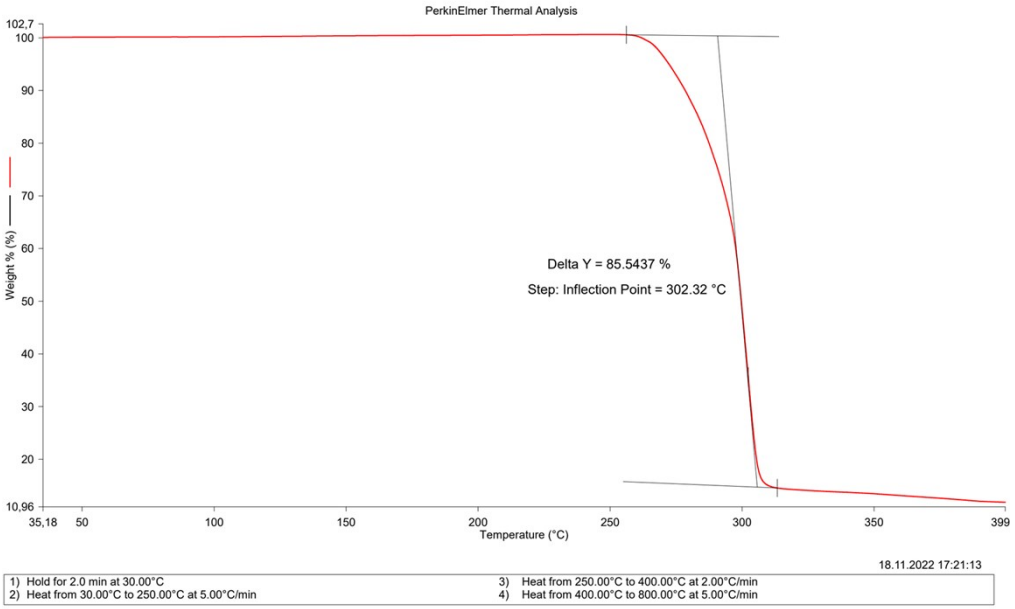

Fig. S11. The thermogravimetric analysis of TePrAClO4